Photonic-structured TiO_2 for high-efficiency, flexible and stable Perovskite solar cells

Sirazul Haque, Manuel J. Mendes*, Olalla Sanchez-Sobrado, Hugo Águas, Elvira Fortunato, Rodrigo Martins*

i3N/CENIMAT, Department of Materials Science, Faculty of Science and Technology, Universidade NOVA de Lisboa and CEMOP/UNINOVA, Campus de Caparica, 2829-516 Caparica, Portugal

**Corresponding authors: mj.mendes@fct.unl.pt , rm@uninova.pt*

Abstract

Optical solutions are promising for Perovskite solar cell (PSC) technology, not only to increase efficiency, but also to allow thinner absorber layers (higher flexibility) and improve stability.
This work optimized the combined anti-reflection and scattering properties of two types of light trapping (LT) structures, based on TiO_2 semi-spheroidal geometries with honeycomb periodicity, for application in PSCs with substrate configuration and different perovskite layer thicknesses. Their optically lossless material (TiO_2) allows the structures to be patterned in the final processing steps, integrated in the cells' top *n* contact, therefore not increasing the surface area of the PV layers and not degrading the electric performance via recombination. Therefore, this strategy circumvents the typical compromise of state-of-the-art LT approaches between optical improvements and electrical deterioration, which is particularly relevant for PSCs since their main recombination is caused by surface defects.
When patterned on the cells' front, the wave-optical micro-features composing the LT structures yield up to 21% and 27% photocurrent enhancement in PSCs with conventional (500nm thick) and ultra-thin (250nm) perovskite layers, respectively; which are improvements close to those predicted by theoretical Lambertian limits. In addition, such features are shown to provide an important encapsulation role, preventing the cells' degradation from UV penetration.

Keywords: Photovoltaics, Photonics, Perovskite Solar Cells, Light Trapping, UV Stability Improvement

1. Introduction

Nowadays, photovoltaics (PV) industry is moving towards ultra-thin and low-cost solar cells for consumer-oriented electronic products with high intrinsic mechanical flexibility [1–3]. To achieve such challenging goal, nano/micro-structured photonic elements in the wave-optics regime are a promising solution, capable of capturing and trapping light within the cells' absorber, thus allowing the reduction of its thickness while boosting efficiency.

On the other hand, the organic-inorganic hybrid halide Perovskite solar cells (PSCs) have received enormous attention in recent years due to their highly promising physical properties for opto-electronics (e.g. PV, LEDs) such as: high absorption coefficient and cross section [4,5], ambipolar charge transport [6,7], and long electron–hole diffusion lengths (above 175 μm) in the single-crystalline phase [8–11]. In the thin film solar cell field, Perovskite-based materials have proven to be highly promising, given their fastest growing efficiency from ~3.8% in 2009 to > 22.1% in 2017 [12–21]. Despite impressively high efficiencies, PSCs face challenges, such as reduced durability which prevents them from competing with established technologies; and there is still room for tailoring charge carrier recombination, both in the perovskite and at the interfaces in the device, to increase performance. For instance, the carrier diffusion lengths in state-of-the-art PSCs based in methylammonium lead iodide ($MAPbI_3$) are on the order of 100 nm, chiefly due to the polycrystalline structure of the solution-processed perovskite films [22], therefore devices with an ultra-thin perovskite active layer (below the typical 500 nm thickness used) could be beneficial for reducing the recombination losses.

Optical solutions are promising to improve not only the PSCs efficiency, by allowing physically thinner but optically thicker devices, but also their market applicability by enabling higher device flexibility due to the reduced thickness. The conventional best-performing PSCs exhibit high transparency in the near-infrared (NIR), thus are only able to exploit a reduced portion (about half) of the solar spectrum [23]. The lower the Perovskite thickness used the more challenging it becomes for optical strategies to compensate the losses in light absorption, mainly at the longer visible-NIR wavelengths [24]. In addition, the application of such strategies in PV is conditioned by other factors, such as maintaining the electrical performance and compatibility with low cost and large area fabrication.

Recent findings in photonics report possibilities to manipulate light in ways that greatly exceed traditional geometrical optical limits, enabling pronounced broadband light trapping (LT) within thin film solar cells [25–27]. The LT approaches conventionally employed in wafer-based cells are based on textured rear/front surfaces, which provide: 1) anti-reflection, via geometrical refractive-index matching by the front facets, improving the short-wavelength (above absorber bandgap) photocurrent; and 2) light scattering, which increases the longer-wavelength (near-bandgap) absorption, via optical path-length amplification and coupling with waveguide modes

confined within the cells structure [28,29]. However, when applied in thin film cells, the size of the textures for thin absorber layers has to be much reduced, which lowers the LT effects [30,31]. Nonetheless, the main disadvantage is that texturing increases roughness (hence surface area) and defect density in the PV material, which deteriorate its electric transport via carrier recombination. This can be a particularly crucial drawback for PV devices whose carrier lifetime is chiefly limited by interfacial recombination/trapping, as has been shown to be the case for PSCs [32].

Several alternative approaches have been tested to increase the light harvesting of PSCs [35,36], for instance by applying ultra-thin textures to the perovskite absorbers [33,34] or the substrate [35,36], applying ray optics by prism arrays [37], microlens [38] or nanocone [39,40] arrays, plasmonic nanoparticles [41–43], light grating-coupled surface plasmon resonances [44] and embedding TiO_2 nanoparticles into the mesoporous TiO_2 layer [45]. However, most of these approaches also require nano/micro-structuring the Perovskite layers, thereby imposing a severe compromise between optical benefits and electrical deterioration; and none has yet led to efficiency enhancements superior to the state-of-the-art of optimized periodic texturing in thin film silicon-based cells [46].

This work investigates front-located wavelength-sized LT structures patterned on top of PSCs, operating in the wave-optics regime, which have been demonstrated to provide pronounced anti-reflection and scattering effects in thin film silicon PV [2,47]. Since they do not require structuring the PV layers, this is a much more promising option to increase the optical performance of thin film cells without increasing their roughness [25,26,46,48]. For that, an inverted (substrate-type) PSC architecture is considered here, where the light enters through the cell side and not from the transparent substrate (as in conventional PSCs). Besides enabling the application of the PSCs in a much broader range of substrates (e.g. with flexible opaque materials), this inverted configuration can also be directly integrated onto multi-junction stacks to realize higher efficient tandem devices (e.g. Perovskite on Si or on GIGS) [49–51].

The wave-optical structures developed in this work for inverted PSCs are based on high-index dielectric (TiO_2) micro-scale features, with semi-spheroidal geometries, which are shown to assist in three fundamental points of PSC technology:

1) *Efficiency enhancement* – the broadband absorption gain caused by optimized LT features can pronouncedly improve the photocurrent. Besides, their optically lossless material (TiO_2) allows them to be patterned in the final processing steps, on top of the already-completed cell, therefore not increasing the roughness or surface area of the PV layers and not degrading the electric performance via recombination. This is particularly relevant for PSCs, since their main recombination mechanism is caused by surface defects [32], and due to the fact that they are usually deposited by spin-coating techniques, so the uniformity and electronic properties of the patterned layers are substantially improved when coated on flat surfaces.

2) *Broader applicability due to higher device flexibility* - the absorption enhancement caused by the LT features allows reducing the Perovskite absorber thickness, which enables improved bendability and cost reduction [1,52,53].

3) *Higher stability against UV light degradation* – one of the main issues of PSCs is degradation upon UV exposure [54,55]. The use of UV blocking layers has been attempted to circumvent this issue, with the drawback of decreasing the light absorption in the Perovskite and, thus, lowering the efficiency [54,56]. Here, the front-coated LT structures are shown to act as highly effective UV-blocking layers, able to protect the underneath sensitive device layers from UV exposure, while improving light absorption at longer wavelengths and, thus, increasing efficiency.

2. Ray optics analysis

The analytical Lambertian light trapping (LT) formalism has been used to determine the limit of maximum absorption in a slab of arbitrary thickness, in the geometric optics regime [57]. This is attained with an ideally rough surface where the incident light is randomly scattered, which can increase the average absorption in the slab by a factor of $4n^2$ compared to flat surfaces in the limit of weak absorption [29], where n is the real part of the refractive index of the slab. For a Perovskite with n~2.5, the $4n^2$ limit means that the path length can be increased by a factor of ~25.

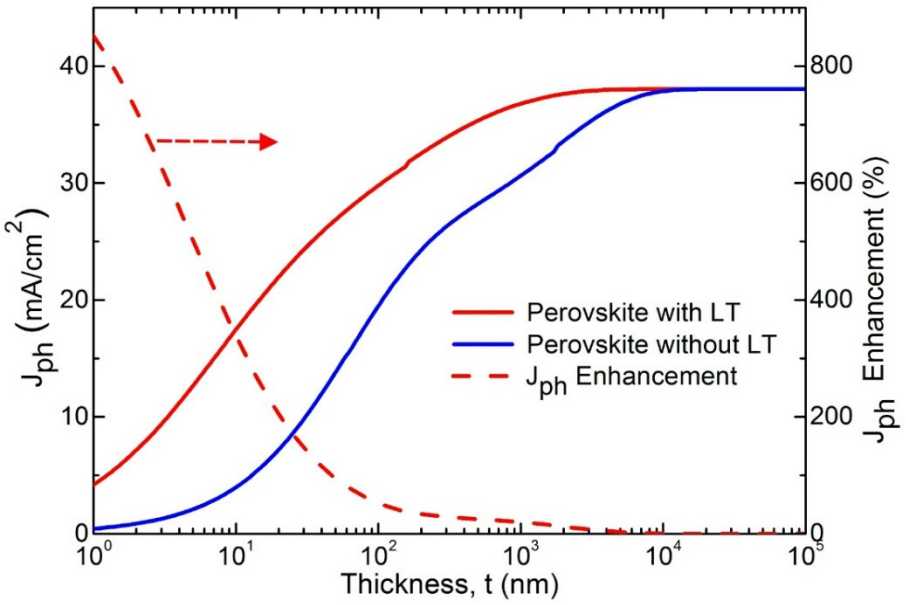

Figure 1: Lambertian theoretical analysis of LT in Perovskite solar cells, in the geometrical optics regime. The maximum photocurrent (J_{PH} – *solid lines*) and J_{PH} enhancement (*dashed line*) are shown as a function of the Perovskite film thickness, for the case with a Lambertian scattering surface (with LT) relative to a flat surface without LT. The thinner the Perovskite film the lower is the maximum J_{PH} but the higher is the attainable enhancement with LT. The wavelength range considered for the calculations was 300-1000 nm.

Such ray optics formalism was further developed to consider the full absorption by a slab with an arbitrary complex refractive index spectrum, allowing to estimate the photocurrent density (J_{PH}) enhancement that can be produced on the absorber with the implementation of Lambertian LT [58,59]. Figure 1 shows the results of such calculation for the case of Perovskite absorbers with distinct thickness, considering that their back surface is coated with a perfect reflector and the front surface has an ideal Lambertian LT texture that disperses light rays at random angles towards the Perovskite [48]. For the two Perovskite thicknesses (250 and 500 nm) analyzed in this work, the limiting J_{PH} enhancements in the ray optics approximation are 31% and 25%, respectively. Such LT limits are only valid in the regime of geometric optics, and therefore are not applicable to the wave-optics regime of the thin film structures analyzed in this work where light interference effects play a major role. Nevertheless, the Lambertian results of Figure 1 can still provide a reasonable first-order prediction of the attainable J_{PH} values in PSCs improved with optimized LT, as the interference effects are mainly important for single wavelength calculations while the J_{PH} results from an integration over the solar spectrum that manipulates interference peaks.

3. Numerical Method and Simulated Structures

The simulations of the electromagnetic field distribution in the thin film solar cell structures were carried out using a 3D Finite Difference Time Domain (FDTD) solver [60]. This is one of the preferential techniques to determine electromagnetic solutions in the wave-optics regime, specifically for PV light management [48,61], since it is conceptually simple, versatile, and can accurately determine all the optical effects at play. Besides, since the computations are performed in the time-domain, the solutions can cover a broad frequency range over a single simulation run. The complex refractive index spectra of the materials composing the structures were taken from experimental data and are plotted in Section S1 of Supplementary Material (SM). The Perovskite solar cell (PSC) structure is composed of 5 layers coated on a substrate in the following order (see Figure 2): rear contact/mirror layer (silver, Ag), hole transport material (HTM made of Spiro-OMeTAD), Perovskite absorber (methylammonium lead iodide, $CH_3NH_3PbI_3$), electron transport material (ETM made of TiO2) and front transparent contact (TCO made of ITO). The spectra of the refractive indices considered for all materials are given in section S1 of SM.

The FDTD computations are performed in a 3D unit cell corresponding to one period of the hexagonal array of the photonic features placed on the PSCs. The incident plane wave source is placed in the air medium and propagates downwards along the *z*-direction, perpendicularly to the solar cell. Perfect Matching Layers (PML) are applied at the finite *z* boundaries of the unit cell, to avoid reflections of outgoing waves. Along the *x* and *y* direction, periodic boundary conditions (BCs) are used to model the infinite periodicity of the structures. Here, due to the symmetries of

the system at normal incidence, symmetric and anti-symmetric BCs are employed which allow simulating only one quadrant of the unit cell. Sets of convergence tests were performed to determine the correct mesh size and number of PMLs [2,48].

The illuminating source bandwidth is 300-1000 nm, since the AM1.5 solar photon flux outside this wavelength range is small and corresponds to the most significant portion of the photocurrent spectrum of PSCs. The power absorbed per unit volume (P_{ABS}) in each element of the structures is given by the resulting electric field distribution established in its material:

$$P_{ABS} = \frac{1}{2}\omega\varepsilon''|\boldsymbol{E}|^2 \qquad (1)$$

where $|\mathbf{E}|^2$ is the electric field strength, ω is the angular frequency of the light and ε" is the imaginary part of the dielectric permittivity. P_{ABS} is normalized by the energy source to obtain the absorption density (p_{ABS}, units of m^{-3}). The absorption of light with a certain wavelength (λ) is calculated by integrating p_{ABS} along the absorber volume: $Abs(\lambda) = \int p_{ABS}(\lambda)dV$. The number of photons absorbed per unit volume and per unit time is the photon absorption rate: $g(\omega)=P_{ABS}/E_{PH}$; where $E_{PH}=\hbar\omega$ is the photon energy. Here we assume that each absorbed photon excites one electron-hole pair, so g is equivalent to the optical generation rate. As the illumination is given by a broadband source, characterized by a spectral irradiance (instead of a power density), the E-field is replaced by an electric field spectral density such that its intensity, $|\mathbf{E}|^2$, becomes with units of $V^2m^{-2}Hz^{-1}$. In this way, g is generalized to a spectral generation rate (in units of $m^{-3}s^{-1}Hz^{-1}$) such that the total generation rate (G, units of $m^{-3}s^{-1}$) is calculated by integrating over the frequency range of the source bandwidth: $G= \int g(\omega)d\omega$ [60].

Since we are primarily concerned with the optical rather than the electrical transport properties of the solar cells, an internal quantum efficiency equal to one is also assumed (i.e. every photon absorbed in the Perovskite generates carriers collected by the contacts). As such, J_{PH} is determined by integrating the absorption in the Perovskite layer, convoluted with the solar power spectrum AM1.5 ($I_{AM\ 1.5}$, units of $Wm^{-2}m^{-1}$), along the computation wavelength range (300-1000 nm):

$$J_{ph} = e\int \frac{\lambda}{hc} Abs(\lambda)\, I_{AM1.5}(\lambda)d\lambda \qquad (2)$$

Where e is the electron charge, h is the Planck constant and c is the free space light velocity. This spectrally-integrated J_{PH} can be considered as an upper limit corresponding to the ideal case of no electrical losses, and is taken here as the figure of merit to optimize the performance of the photonic structures.

Using a particle swarm optimization algorithm (PSO) [60] in the FDTD programs, a complete screening of the geometrical parameters of the LT elements (indicated in Figure 2) was performed, searching for the set of parameters that produces the highest J_{PH}. The algorithm iteratively adjusts the geometry of the TiO_2 LT structures, and thickness of the TCO and ETM layers, to maximize absorption in the Perovskite region, minimizing optical losses (ie total reflection and absorption

occurring in the TCO and TiO_2 materials). Population-based stochastic optimization techniques, such as the PSO, are preferred when operating with complex physical systems, as in the current wave-optical regime, where there is a strong correlation between all the parameters of the structures, making it practically unfeasible to precisely determine the global maximum of any figure of merit by simple sequential scanning of the parameters.

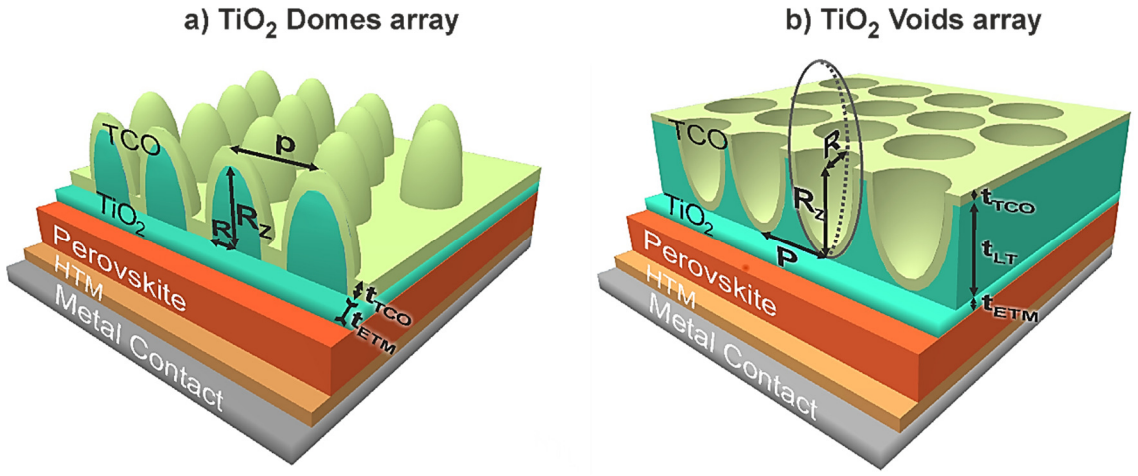

Figure 2: Sketch of both types of LT structures analyzed in this work, composed of TiO_2 features integrated on the ETM of the PSCs. The PSCs have a substrate-type layer configuration, in which light comes into the devices from the film side. The LT structures consist in a hexagonal array (with pitch p) of vertically aligned semi-prolate features with radii R and R_Z, respectively along the in-plane direction and illumination axis. The parameters (R, R_Z, p, t_{TCO}, t_{ETM}) for the structure (a) and the parameters (R, R_Z, p, t_{TCO}, t_{LT}, t_{ETM}) for the structure (b) considered for optimization are indicated by the arrows. At normal incidence, light impinges from the top along the spheroids' axis of revolution (z). The rear side of the perovskite is coated with a 150-nm-thick Spiro-OMeTAD layer (HTM) and a 80 nm silver layer (metal contact).

4. Optimized photonic-enhanced Perovskite solar cells

As demonstrated theoretically [2,48], the absorption enhancements attained with wave-optical elements on the cells' front are maximized when the complex refractive index ($N=n+ik$) of their dielectric material has lowest imaginary part (k) at the sunlight wavelengths (to minimize parasitic optical losses), and has a real part (n) as close as possible to that of the underlying absorber (e.g. n~2.5 in Perovskite and n~4 in Si) to improve anti-reflection via geometric index matching. High values of n also boost the light scattering performance of the photonic features, since their scattering cross section increases with n. TiO_2 was shown to be one of the preferential materials to fulfill such requirements in thin film silicon solar cells [47,48], but it can perform even better in PSCs since its n~2.4-2.7 is much closer to that of Perovskite (see plots of refractive indices in Fig. S1 of SM). Therefore, TiO_2 was the material considered for the photonic structures optimized

in this work for PSCs (sketched in Figure 2). In fact, conventional PSCs already use compact (~20-30 nm thick) and/or mesoporous (~200-400 nm thick) TiO_2 layers as electron transporters, so the TiO_2 LT structures should be incorporated on such layers as a continuation of the cells' ETM. Due to the low electric conductivity of TiO_2, it must be coated with a transparent conductive oxide (TCO) acting as the front (*n*-type) electrode. Here we consider the most commonly used TCO composed of indium tin oxide (ITO) deposited conformally over the TiO_2 features.

The optimization method described in section 3 was applied to find the set of geometrical parameters of the two types of geometries depicted in Figure 2 that maximize the generated photocurrent in the underlying PSC. Here we consider a substrate-type PSC layer structure due to two main aspects:

1) To maintain the electrical performance (prevent increase of roughness and consequent recombination) of the PSCs after implementing the LT structures at the last processing steps.
2) To allow the integration of the devices on a wider range of substrates, including opaque ones, such as rigid (e.g. roof and wall tiles for BIPV, metallic coverage of vehicles, etc.) or flexible (e.g. PI, metal foils, fabrics [62], plastics [63,64], paper-based [65]) materials.

LT can play a crucial role in the development of flexible solar cells, since it allows decreasing the cells' thickness without photocurrent loss, or even enhancing it as shown here. To explore that, the photonic structures of Figure 2 were optimized for both the conventional Perovskite layer thickness (500 nm) used in state-of-art devices, and for half that thickness (250 nm) to be applied in flexible devices. Note that a reduction of the absorber layer to half can enable a decrease up to about four times in the device flexural rigidity [63].

The geometry of the photonic structures is an hexagonal array of semi-spheroidal dome (Figure 2a) or void (Figure 2b) elements, as these are similar structures to those that can be fabricated by industrially-attractive patterning techniques such as colloidal lithography [2,47,66], which is an inexpensive soft-lithography method that can engineer any structure with nano/micrometer resolution and high uniformity throughout large areas [47]. The geometrical parameters considered for optimization are indicated in Figure 2. These are taken as variables by the PSO algorithm that iteratively searches for the best set of parameters that maximizes the photocurrent (J_{PH}, eq. 2) produced in the PSC, considering reasonable boundaries for their domains.

Table 1 presents the main outcomes of the optimization studies performed in this work, indicating the best parameters and the corresponding maximum J_{PH} values attained. The first line presents the theoretical *Lambertian* limits of geometrical optics, as described in section 2 (see Figure 1). The second line presents the optimized values for the thicknesses of the two flat layers of TiO_2 and TCO (composed of ITO) coated over the Perovskite, acting as a planar double-layer anti-reflection coating (ARC), which is the reference LT case considered here for comparison with the results attained with the two types of TiO_2 micro-structures presented in the two last lines of Table

1 and sketched in Figure 2. The results and discussion of the optimization studies for the planar reference LT structures (ARC cases) are presented in section S2 of SM.

Table 1: Maximum J_{PH} values attained for the optimized LT structures placed on the two distinct PSCs, with 250 or 500 nm perovskite layer thickness, considered in this work. The geometrical optimization parameters (R, R_Z, p, t_{TCO}, t_{ETM}) and (R, R_Z, p, t_{TCO}, t_{LT}, t_{ETM}), respectively for the Dome and Void structures, are defined in Figure 2. The results are compared with the reference ARC-patterned cases, as well as with the theoretical limits in the regime of geometrical optics attained with a *Lambertian* scattering surface.

Light Trapping Structure	Absorber: **250 nm Perovskite layer**		Absorber: **500 nm Perovskite layer**	
	Optimal Parameters	J_{PH} | $J_{PH\_VIS\text{-}NIR}$ (mA/cm^2)	Optimal Parameters	J_{PH} | $J_{PH\_VIS\text{-}NIR}$ (mA/cm^2)
Lambertian surface	-	**33.3 | 32.0**	**-**	**35.3 | 34.1**
Planar ARC *(Figure S3)*	t_{TCO} = 50 nm t_{ETM} = 20 nm	**22.6 | 21.1**	t_{TCO} = 76 nm t_{ETM} =20 nm	**25.9 | 24.9**
Dome structures *(Figure 3)*	t_{TCO} = 50 nm t_{ETM} =159.1 nm R = 785.2 nm Rz = 1755 nm p = 1825.6 nm	**28.0 | 27.7**	t_{TCO} = 50 nm t_{ETM} = 132.7 nm R = 502.6 nm Rz = 1007 nm p = 1347.1 nm	**30.6 | 30.3**
Void structures *(Figure 4)*	t_{TCO} = 63.6 nm t_{ETM} = 20 nm R = 401.2 nm Rz = 1792 nm t_{LT} = 656.2 nm p = 882.7 nm	**28.6 | 28.3**	t_{TCO} = 62.3 nm t_{ETM} = 93.2 nm R = 388.0 nm Rz = 820.8 nm t_{LT} = 404.6 nm p = 865.3 nm	**31.3 | 30.8**

4.1 Optimal dome front structures

Figure 3 presents the results attained with the optimized set of geometrical parameters of the hexagonal array of TiO_2 half-spheroids, shaped like domes as shown in Figure 2a, and of the thicknesses of the flat ETM layer (t_{ETM}), placed between the domes and Perovskite, and front contact (t_{TCO}) coating the structure. These results (red curves) are compared to those of the planar reference cells (blue curves) with the optimized double-layer ARC, for the two Perovskite absorber thickness (250 and 500 nm) considered in this work.

The standard planar cell structure, with 500 nm Perovskite layer, exhibits high absorption in the Perovskite along 375 to 750 nm wavelengths. Above 750 nm there is an abrupt absorption drop of about 92%, occurring at the bandgap of the Perovskite material. In the case of the thinner (250 nm) Perovskite, there is a first smaller absorption drop at 600 to 750 nm wavelengths, and then above 750 nm there is a larger absorption drop at the bandgap of nearly 93%. The incorporation of the dome-like LT structures improves the optical performance of the cells mainly by decreasing

such drops in absorption observed for the planar PSCs, namely in the visible range (600 to 750 nm wavelengths) for the thinner (250 nm) Perovskite and in the NIR (>750 nm wavelengths) for both the 250 and 500 nm Perovskite absorbers.

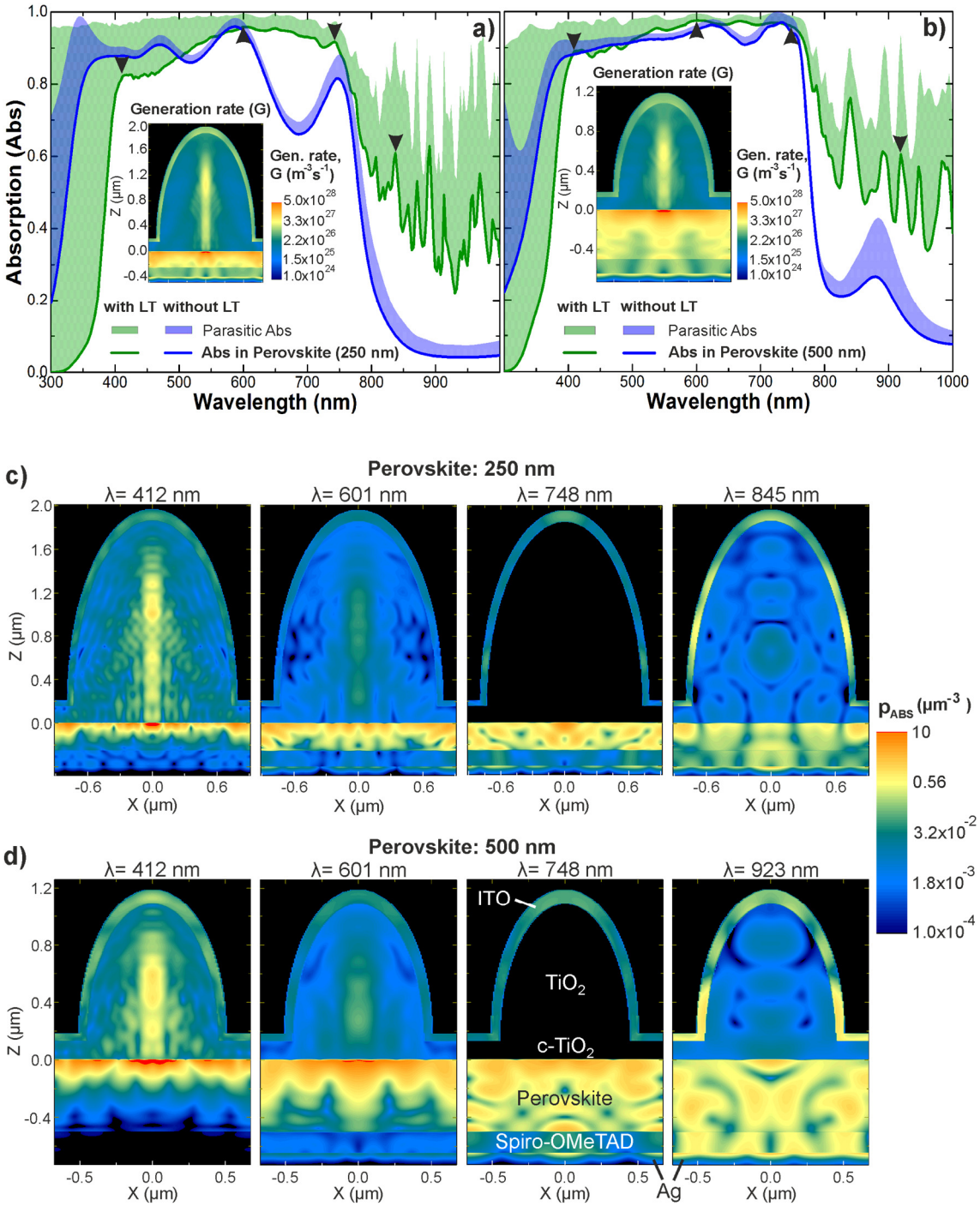

Figure 3: a,b) Absorption spectra attained with the optimized LT structures sketched in Figure 2a, composed of half-spheroidal domes (*green lines*, row 4 of Table 1), and with the reference cases of a cell with an optimized anti-reflection coating (*blue lines*, row 3), for Perovskite absorber layers with distinct thickness: a) 250 nm and b) 500 nm. Each graph shows the absorption occurring in Perovskite (*solid lines*) and the parasitic absorption in the other materials (*colored regions* above the lines). The inset profiles show

the log-scale distribution of the corresponding total generation rate, G, along the xz cross-sectional plane of the structures passing by the spheroid center. **c,d)** Log-scale distributions of the absorption density, p_{ABS}, along the same xz plane of the structures, at the wavelengths of the peaks marked by the arrows in a) and b) respectively for the half-spheroids array on the 250 nm (c) and 500 nm (d) thick Perovskite absorbers.

The enhancement in the visible range is due to a better light incoupling towards the Perovskite layer provided by the front TiO_2 structures, via two main mechanisms: 1) Anti-reflection due to the geometrical index matching caused by the cone-like shape of the TiO_2 features, which is favored by the proximity between the values of the real part of the refractive indices of TiO_2 and Perovskite (plotted in section S1 of SM). In fact, at a wavelength of approximately 600 nm, the n~2.41 of TiO_2 is equal to that of the Perovskite material, which highly contributes to the maximum of absorption (Abs= 0.96 and 0.98, respectively for Figure 3a,b) in the Perovskite occurring near such wavelength. 2) Near-field forward-scattering, since the domes act as micro-lenses creating an intense electric-field focus in the vicinity below their bottom surface, which is vital to confine the light specially in the thinner Perovskite layer. This effect is mostly relevant for wavelengths smaller than the dimensions of the scattering elements, in this case in the UV-visible range, as observed by the highly intense regions of localized electric field in the generation profiles of Figure 3a,b and in the p_{ABS} profiles of Figure 3c,d for the 412 and 601 nm wavelengths. The enhancements observed in the NIR range are mainly caused by the strong far-field scattering effects of the TiO_2 domes, owing to their optimized shape and high real part of the refractive index, which increase the absorption in the Perovskite layer via optical path length amplification, by diverting the vertically incident light to more horizontal directions along the layers' plane, and coupling with waveguided modes trapped in the cell layers. This is evidenced by the distributed regions of higher p_{ABS} (hot-spots), observed in the profiles of Figure 3c,d for wavelengths >700 nm, which result from constructive and destructive interference between the light waves traveling along the incidence direction and the scattered light that travels along the plane of the cell layers suffering multiple reflections from the top surface and back reflector. These can be seen as 3D Fabry-Perot resonances, compared to the 1D Fabry-Perot resonances in planar layer structures, which lead to the sharp NIR peaks of absorption enhancement present in Figures 3a,b.

The light absorption in the Perovskite is the only one that can generate photocurrent, so the absorption in the other materials is referred as parasitic absorption, since it corresponds to optical losses not translated into electrical output by the cell. The main parasitic absorption in the planar references occurs chiefly in two spectral regions: 1) in the UV (300-400 nm wavelengths) since the imaginary part of the refractive index (k) of ITO and TiO_2 increases abruptly for wavelengths below 400 nm (see Figure S1 in SM); 2) in the NIR (>800 nm wavelengths) due to the free carrier light absorption in the ITO, which leads to an increase of its k for the longer wavelengths, and

absorption at the cell rear in the HTM (Spiro-OMeTAD). These parasitic losses can be observed in the generation rate (Figure S3a,b) and p_{ABS} profiles (Figure S3c,d) presented in SM for the planar reference cells. In the structures with the TiO_2 domes the parasitic absorption occurs for the same reasons, but for shorter wavelengths it is more pronounced along a broader range (300-500 nm) extending to the visible spectrum, due to absorption by the LT features at the cells' front as seen in the generation profiles of Figure 3a,b and p_{ABS} profiles of Figure 3c,d at 412 nm wavelength. In the NIR, it can be seen from the plots of Figure 3c,d that the parasitic absorption happens mainly in the top ITO and in the bottom HTM, as occurred in the planar cells.

The severe parasitic absorption caused by the front TCO explains why the optimization algorithm converged to the minimum allowed thickness (t_{TCO}=50 nm) for the domes LT structures (see Table 1). Contrary to the planar cases, the anti-reflection LT effects caused by the domes structures are chiefly given by the geometrical index matching that they provide on the cell front. So, the TCO layer does not provide any beneficial optical contribution in these structures, and the thinner it is the better. However, a TCO layer with at least 50 nm thickness must be considered for electrical purposes, as it acts as the front *n*-electrode. On the other hand, the thickness of the underlying flat ETM layer (t_{ETM}~133-159 nm) converged to much higher values that those (t_{ELT}=20 nm) of the planar references, thus revealing that it is optically favorable to establish a separation between the bottom surface of the semi-spheroidal domes and the top surface of the Perovskite layer, in order to provide better light incoupling and confinement in the absorber.

4.2 Optimal void front structures

The results of the optimized LT structures based on spheroidal voids (sketched in Figure 2b) are presented in Figure 4. Despite the considerable differences in geometry, the absorption spectra and generation profiles of Figure 4a,b produced with the voids array are similar to those of Figure 3a,b attained with the domes. However, the voids provide a slightly higher absorption mainly at short visible wavelengths (400-500 nm) due to better anti-reflection, and in the NIR region due to improved scattering, both in the 250 and 500 nm Perovskite absorbers, thus leading to higher values of J_{PH} (last row of Table 1). The p_{ABS} profiles shown in Figure 4c,d reveal that the voids structure generally creates a more uniform spatial distribution of the absorption enhancement throughout the volume of the Perovskite layer, while the domes array generates more localized (confined) regions of highest electric field intensity due to the focal effect of their micro-lens shape. This explains the better performance of the voids structure for light scattering, i.e. bending of light waves, which justifies the higher values of absorption at the longer NIR wavelengths.

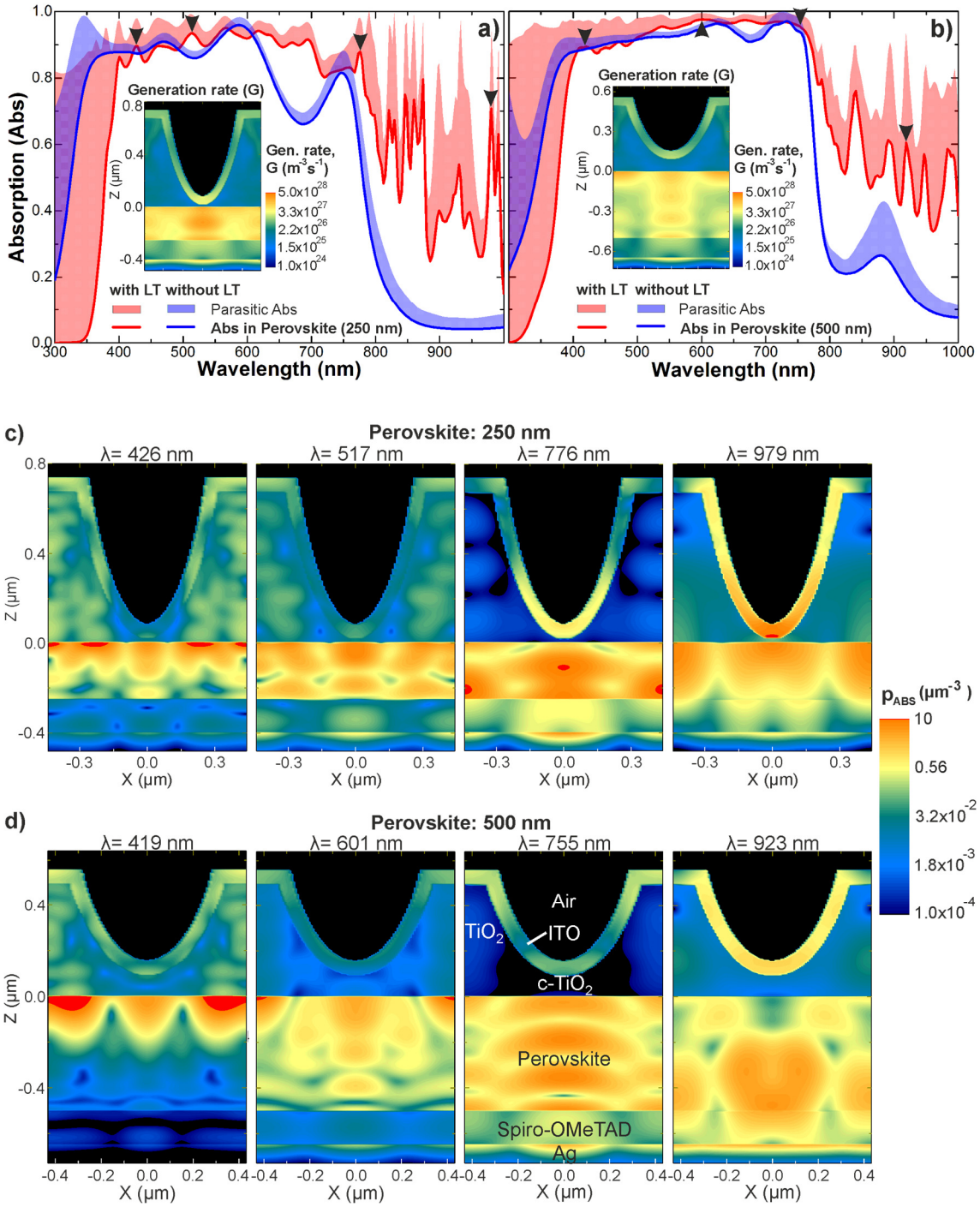

Figure 4: Same as Figure 3 but for the LT structures sketched in Figure 2b, composed of semi-spheroidal voids in the TiO_2 film. **a,b)** Absorption spectra attained with the optimized LT structures (*green lines*, row 5 of Table 1), and with the planar reference ARC cases (*blue lines*, row 3), for Perovskite layers with a) 250 nm and b) 500 nm thickness. Each graph shows the absorption occurring in Perovskite (*solid lines*) and the parasitic absorption in the other materials (*colored regions* above the lines). The inset profiles show the log-scale distribution of the corresponding generation rate, G, along the xz cross-sectional plane of the structures. **c,d)** Log-scale distributions of the absorption density, p_{ABS}, along the same plane, at the wavelengths of the peaks marked by the triangles in a) and b) respectively for the voids array on the 250 nm (c) and 500 nm (d) thick Perovskite.

In the voids case, the optimal TCO thicknesses (t_{TCO}) indicated in Table 1 are higher than those of the domes, since such front contact now improves the anti-reflection in the flat regions between voids on the top surface. On the other hand, the thicknesses of the flat ETM (t_{ETM}) are smaller, since this layer plays a lesser role for geometric index matching in this structure.

For the voids and domes structures, the optimized lateral (R) and vertical (Rz, t_{LT}) dimensions of the TiO_2 features are larger for the thinner 250 nm Perovskite, as the thinner the absorber the higher are the requirements for scattering: it needs to provide stronger path length enhancement for a broader wavelength range (i.e. extending to shorter wavelengths than those of thicker absorbers). This is achieved chiefly by enlarging the lateral sizes of the scattering elements, thus yielding higher scattering cross sections. Nevertheless, the optimal vertical size must also increase with the lateral size to maintain effective geometrical index matching provided by the front features, and consequent broadband anti-reflection. Since the thicker 500 nm Perovskite has a lower need for scattering, the optimized design of the TiO_2 features converged to smaller dimensions and to larger array pitch (p) to also minimize the parasitic absorption of the LT structures.

5. Discussion

The main distinguishing advantage of the LT schemes designed here, over the conventional texturing/structuring-based LT approaches mentioned in the Introduction, is that they can remarkably enhance light harvesting without creating roughness in the thin PV layers. This is because the photonic elements are placed on top of the unstructured planar solar cells. Thus, they do not increase the amount of defect states, that can strongly contribute to electrical deterioration particularly in PSCs [67,68], allowing the geometry of the photonic structures to be fully optimized for maximum LT without constraints concerning the degradation of the electrical performance of the devices. Consequently, the voltage and fill factor of the cells is expected to be maintained (even possibly increased), while substantially boosting the photocurrent. Therefore, the efficiency gains resulting from the incorporation of the optimized LT structures are expected to be similar to their corresponding J_{PH} enhancements.

An important aspect of the absorption curves of Figures 3 and 4 resulting from the incorporation of LT structures, is that the strongest parasitic absorption occurs in the UV range (300-400 nm) mainly due to the relatively large volume of the photonic structures and the significant k of their TiO_2 material below 400 nm wavelengths (see Figure S1 in SM). Nevertheless, such optical losses in the UV can actually be quite advantageous for the stability of PSCs, as one of the main factors for the poor lifetime of this type of PV devices is their severe degradation upon UV illumination. The mechanism responsible for UV light degradation in PSCs is attributed to the photocatalytic activity of TiO_2 occurring in the interface between the ETM and the Perovskite layer. Upon prolonged UV light exposure, the photo-generated holes react with the oxygen radicals adsorbed

at surface oxygen vacancies, which become deep traps within the Perovskite increasing charge recombination [69]. Therefore, blocking UV photons from entering the PSCs has proven to be beneficial, yielding longer time of stabilized high efficiency [70,71]. As such, here the TiO_2 structures advantageously act as a UV-protective layer that, at the same time, enhances the absorption of visible and NIR photons in the Perovskite absorber, thus leading to overall J_{PH} gains while contributing to the device robustness in standard sunlight exposure conditions.

Figure 5 represents such gains, relative to the optimized planar reference cells (see Section S2 in SM), determined from the J_{PH} values of Table 1 for the two types of LT geometries explored in this work (domes and voids) and both Perovskite thicknesses (250 and 500 nm). Besides, to analyze the aspect described in the previous paragraph, we also represent the enhancements considering the photocurrent density values ($J_{PH\_VIS\text{-}NIR}$) shown in Table 1 determined from photon absorption in the Perovskite outside the UV range (i.e. restricting the integral of eq. 2 to the 400-1000 nm wavelength range, instead of the total 300-1000 nm range of Figures 3 and 4). Such $J_{PH\_VIS\text{-}NIR}$ gains can be regarded as the improvements that would be achieved considering PSCs with a UV-blocking filter for better stability.

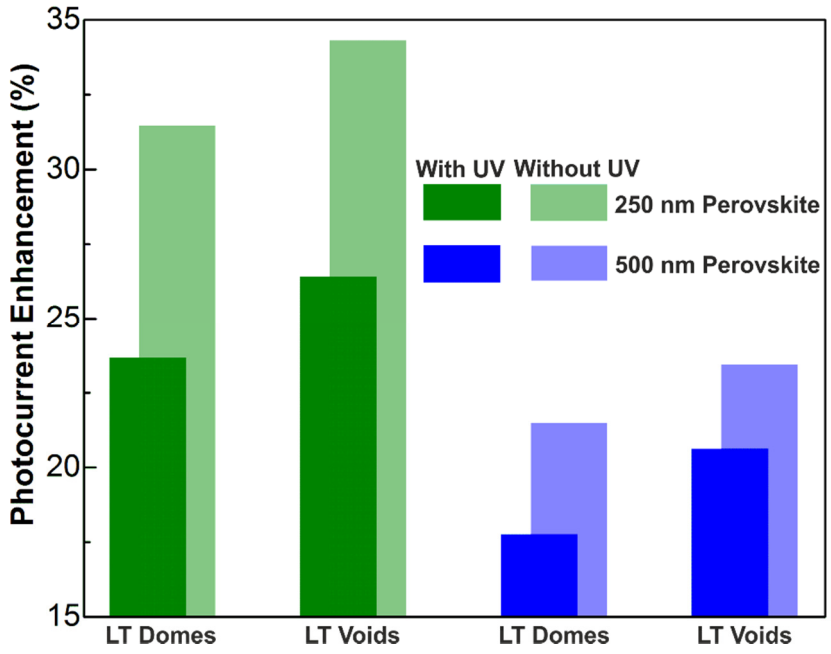

Figure 5: Photocurrent enhancements attained with the optimized photonic structures (last 2 rows of Table 1) analyzed in section 4, relative to the planar double-layer ARC references (row 2 of Table 1 and Section S2). The absolute J_{PH} values were calculated by integrating the spectral absorption (eq. 2) in the UV-VIS-NIR wavelength range (300-1000 nm – *with UV*) and only in the VIS-NIR (400-1000 nm – *without UV*), for both Perovskite thicknesses (250 and 500 nm) analyzed in this work.

Figure 5 shows that the voids array outperforms the domes, as the present PSCs take more profit from the higher degree of light spreading provided by the voids, instead of the higher light focusing effect of the micro-lens shape of the domes. This can be advantageous for practical implementation, since void-like structures can be more straightforwardly fabricated than domes when employing scalable colloidal-lithography (CL) techniques. To form the desired void arrays, the CL processes use hexagonal arrays of colloidal microspheres as mask for the subsequent deposition of any material (in this case TiO_2) in the inter-spaces between the dry-etched spheres [47,72], which results in nano/micro-patterned layers after the spheres lift-off. However, the better performance of LT structures composed of voids relative to domes may not apply to even thinner Perovskite layers that can take more advantage from the higher localization of the electric field enhancement in the ultra-thin Perovskite. This was seen in a previous work of the authors applied to thin film Si cells, in which for 100 nm thin a-Si cells the optimized domes provide higher enhancement than the voids [2].

Although the highest absolute photocurrent values are attained with 500 nm thick Perovskite (30.6 and 31.3 mA/cm^2, respectively with domes and voids), the optimized LT structures on the 250 nm absorber yield the highest enhancements (see Figure 5). The lower the absorber thickness the higher can be the absorption gain provided by optimized LT, as expected from the Lambertian ray optics analysis of Figure 1. The maximum values of the absolute J_{PH} (33.3 and 35.3 mA/cm^2, respectively for 250 and 500 nm thick Perovskites) and LT enhancement (30.6% and 25.2%, respectively) determined with idealized Lambertian surfaces are close but above those attained in this work (see Table 1 and Figure 5), which indicates that there is still room for further improvement of the optical schemes. The main reason for the lower photocurrents attained with the wave-optical structures, relative to the Lambertian limits, is the parasitic losses in the front TCO and TiO_2 materials. Therefore, the J_{PH} values of the optimized geometries would be closer to the Lambertian ones if no TCO was considered on top of the structures, or if distinct materials were investigated with lower extinction coefficient.

The most impactful result shown in Figure 5 is the J_{PH} enhancement (27% with UV and 34.3% within only VIS-NIR) attained with the optimized voids array on the 250 nm thick Perovskite, since it demonstrates an improved device architecture that can allow: 1) higher photocurrent (hence efficiency) relative to conventional planar PSCs with thicker (500 nm) Perovskite layers; 2) a potential 3-fold improvement in the device flexibility due to the thinner absorber, since the flexural rigidity of the cell scales with the third power of its total thickness; 3) a 2-fold reduction in the costs associated to the Perovskite material; and 4) potentially better PSC stability due to the role of the LT structure as a UV-blocking filter. In addition, such enhancement is considerably higher than the state-of-the-art enhancement (14.4% with 300 nm thick Perovskite absorber) achieved thus far using conventional texturing on the FTO/glass substrate [35,53].

6. Conclusions

The high absorption coefficient and direct bandgap at appropriate energy of Perovskite-based materials allow them to act as effective sunlight absorbers in thin film solar cells, thus having less need for absorption enhancement via LT solutions relative to Si-based thin film PV. This explains why there have been little advances so far on photonic strategies applied to PSCs. Nevertheless, the novel optimized photonic designs presented here, based on wave-optical TiO_2 front structures incorporated in the usual TiO_2 ETM of PSCs, are shown to improve substantially the absorption in the Perovskite absorber for wavelengths above 600 nm, due to the strong anti-reflection (mainly in VIS) and light scattering (in NIR) effects. This allows remarkable photocurrent gains, indicated in Figure 5, which should translate into similar efficiency enhancements since the LT structures are patterned over the cells, therefore they are not expected to degrade the electric performance. These enhancements become increasingly pronounced with decreasing Perovskite thickness, thereby allowing thinning the cell absorber while increasing its photocurrent. For instance, the optimized void structures, which were shown to be more optically favorable than the domes, enable a PSC with a thin (250 nm) Perovskite thickness to supply a 28.62 mA/cm^2 photocurrent density, which is 10.3% higher than that (25.95 mA/cm^2) attained with the conventional Perovskite thickness (500 nm) coated with an optimized planar double-layer ARC.

It was also observed that there is a reasonable tolerance of the optimized results with respect to deviations in the geometrical parameters of the LT structures, since 5% variations in the values of each parameter result in <5% relative reduction in J_{PH}. The photocurrent close to the optimum point was seen to be mainly sensitive to the variations in the radius R and pitch p of the LT structures, which are the parameters that chiefly govern the scattering properties.

Lastly, in addition to their strong optical role, the developed front-located LT structures can allow important improvements in the operational stability of Perovskite solar cells. On one hand, their TiO_2 material blocks almost all the UV light from entering the cell, thus protecting the device against degradation from such harmful radiation. On the other hand, the high aspect ratio of the photonic microstructures renders the top surface super-hydrophobic (i.e. water-repellent), allowing water droplets to easily roll-off, carrying away dust or other particles. This can therefore contribute to the outdoor robustness of the device, by improving the cell encapsulation against water ingress and allowing a self-cleaning functionality [73].

Acknowledgements

This work was funded by FEDER funds, through the COMPETE 2020 Program, and national funds, through the Portuguese Foundation for Science and Technology (FCT-MEC), under the

projects POCI-01-0145-FEDER-007688 (Reference UID/CTM/50025), ALTALUZ (Reference PTDC/CTM-ENE/5125/2014) and SUPERSOLAR (PTDC/NAN-OPT/28430/2017). The authors acknowledge partial funding from the European Projects BET-EU (H2020-TWINN-2015, grant 692373) and APOLO (H2020-LCE-2017-RES-RIA, grant 763989). M. J. Mendes and O. Sanchez-Sobrado acknowledge funding by FCT-MEC through the grants SFRH/BPD/115566/2016 and SFRH/BPD/114833/2016, respectively. S. Haque also acknowledges the support from the FCT-MEC through the AdvaMTech PhD program scholarship PD/BD/143031/2018. The authors would like to thank Guilherme Ribeiro, for his assistance with image editing and composition, and Dr. António Vicente for fruitful discussions.

7. References

[1] M. Ye, X. Hong, F. Zhang, X. Liu, Recent advancements in perovskite solar cells: flexibility, stability and large scale, J. Mater. Chem. A. 4 (2016) 6755–6771. doi:10.1039/C5TA09661H.

[2] M.J. Mendes, S. Haque, O. Sanchez-Sobrado, A. Araújo, H. Águas, E. Fortunato, R. Martins, Optimal-Enhanced Solar Cell Ultra-thinning with Broadband Nanophotonic Light Capture, IScience. 3 (2018) 238–254. doi:10.1016/j.isci.2018.04.018.

[3] A. T. Vicente, A. Araújo, M.J. Mendes, D. Nunes, M.J. Oliveira, O. Sanchez-Sobrado, M.P. Ferreira, H. Águas, E. Fortunato, R. Martins, Multifunctional cellulose-paper for light harvesting and smart sensing applications, J. Mater. Chem. C. 6 (2018) 3143–3181. doi:10.1039/C7TC05271E.

[4] M.A. Green, A. Ho-Baillie, H.J. Snaith, The emergence of perovskite solar cells, Nat. Photonics. 8 (2014) 506–514. doi:10.1038/nphoton.2014.134.

[5] S. De Wolf, J. Holovsky, S.-J. Moon, P. Löper, B. Niesen, M. Ledinsky, F.-J. Haug, J.-H. Yum, C. Ballif, Organometallic Halide Perovskites: Sharp Optical Absorption Edge and Its Relation to Photovoltaic Performance, J. Phys. Chem. Lett. 5 (2014) 1035–1039. doi:10.1021/jz500279b.

[6] J.H. Noh, S.H. Im, J.H. Heo, T.N. Mandal, S. Il Seok, Chemical Management for Colorful, Efficient, and Stable Inorganic–Organic Hybrid Nanostructured Solar Cells, Nano Lett. 13 (2013) 1764–1769. doi:10.1021/nl400349b.

[7] G.E. Eperon, S.D. Stranks, C. Menelaou, M.B. Johnston, L.M. Herz, H.J. Snaith, Formamidinium lead trihalide: a broadly tunable perovskite for efficient planar heterojunction solar cells, Energy Environ. Sci. 7 (2014) 982. doi:10.1039/c3ee43822h.

[8] Q. Dong, Y. Fang, Y. Shao, P. Mulligan, J. Qiu, L. Cao, J. Huang, Solar cells. Electron-hole diffusion lengths > 175 μm in solution-grown CH3NH3PbI3 single crystals.,

Science. 347 (2015) 967–70. doi:10.1126/science.aaa5760.

[9] A. Mei, X. Li, L. Liu, Z. Ku, T. Liu, Y. Rong, M. Xu, M. Hu, J. Chen, Y. Yang, M. Gratzel, H. Han, A hole-conductor-free, fully printable mesoscopic perovskite solar cell with high stability, Science (80-.). 345 (2014) 295–298. doi:10.1126/science.1254763.

[10] S.D. Stranks, G.E. Eperon, G. Grancini, C. Menelaou, M.J.P. Alcocer, T. Leijtens, L.M. Herz, A. Petrozza, H.J. Snaith, Electron-hole diffusion lengths exceeding 1 micrometer in an organometal trihalide perovskite absorber., Science. 342 (2013) 341–4. doi:10.1126/science.1243982.

[11] G. Xing, N. Mathews, S. Sun, S.S. Lim, Y.M. Lam, M. Grätzel, S. Mhaisalkar, T.C. Sum, Long-range balanced electron- and hole-transport lengths in organic-inorganic CH3NH3PbI3., Science. 342 (2013) 344–7. doi:10.1126/science.1243167.

[12] A. Kojima, K. Teshima, Y. Shirai, T. Miyasaka, Organometal Halide Perovskites as Visible-Light Sensitizers for Photovoltaic Cells, J. Am. Chem. Soc. 131 (2009) 6050–6051. doi:10.1021/ja809598r.

[13] J.-H. Im, C.-R. Lee, J.-W. Lee, S.-W. Park, N.-G. Park, 6.5% efficient perovskite quantum-dot-sensitized solar cell, Nanoscale. 3 (2011) 4088. doi:10.1039/c1nr10867k.

[14] H.-S. Kim, C.-R. Lee, J.-H. Im, K.-B. Lee, T. Moehl, A. Marchioro, S.-J. Moon, R. Humphry-Baker, J.-H. Yum, J.E. Moser, M. Grätzel, N.-G. Park, Lead Iodide Perovskite Sensitized All-Solid-State Submicron Thin Film Mesoscopic Solar Cell with Efficiency Exceeding 9%, Sci. Rep. 2 (2012) 591. doi:10.1038/srep00591.

[15] M.M. Lee, J. Teuscher, T. Miyasaka, T.N. Murakami, H.J. Snaith, Efficient hybrid solar cells based on meso-superstructured organometal halide perovskites., Science. 338 (2012) 643–7. doi:10.1126/science.1228604.

[16] M. Saliba, T. Matsui, J.-Y. Seo, K. Domanski, J.-P. Correa-Baena, M.K. Nazeeruddin, S.M. Zakeeruddin, W. Tress, A. Abate, A. Hagfeldt, M. Grätzel, Cesium-containing triple cation perovskite solar cells: improved stability, reproducibility and high efficiency, Energy Environ. Sci. 9 (2016) 1989–1997. doi:10.1039/C5EE03874J.

[17] N.J. Jeon, J.H. Noh, W.S. Yang, Y.C. Kim, S. Ryu, J. Seo, S. Il Seok, Compositional engineering of perovskite materials for high-performance solar cells, Nature. 517 (2015) 476–480. doi:10.1038/nature14133.

[18] W.S. Yang, J.H. Noh, N.J. Jeon, Y.C. Kim, S. Ryu, J. Seo, S.I. Seok, High-performance photovoltaic perovskite layers fabricated through intramolecular exchange, Science (80-.). 348 (2015) 1234–1237. doi:10.1126/science.aaa9272.

[19] D. Bi, C. Yi, J. Luo, J.-D. Décoppet, F. Zhang, S.M. Zakeeruddin, X. Li, A. Hagfeldt, M. Grätzel, Polymer-templated nucleation and crystal growth of perovskite films for solar cells with efficiency greater than 21%, Nat. Energy. 1 (2016) 16142. doi:10.1038/nenergy.2016.142.

[20] W.S. Yang, B.-W. Park, E.H. Jung, N.J. Jeon, Y.C. Kim, D.U. Lee, S.S. Shin, J. Seo, E.K. Kim, J.H. Noh, S. Il Seok, Iodide management in formamidinium-lead-halide-based perovskite layers for efficient solar cells., Science. 356 (2017) 1376–1379. doi:10.1126/science.aan2301.

[21] S. Yang, W. Fu, Z. Zhang, H. Chen, C.-Z. Li, Recent advances in perovskite solar cells: efficiency, stability and lead-free perovskite, (n.d.). doi:10.1039/c7ta00366h.

[22] T.M. Brenner, D.A. Egger, L. Kronik, G. Hodes, D. Cahen, Hybrid organic—inorganic perovskites: low-cost semiconductors with intriguing charge-transport properties, Nat. Rev. Mater. 1 (2016) 15007. doi:10.1038/natrevmats.2015.7.

[23] E. Della Gaspera, Y. Peng, Q. Hou, L. Spiccia, U. Bach, J.J. Jasieniak, Y.-B. Cheng, Ultra-thin high efficiency semitransparent perovskite solar cells, Nano Energy. 13 (2015) 249–257. doi:10.1016/J.NANOEN.2015.02.028.

[24] Q. Lin, A. Armin, R.C.R. Nagiri, P.L. Burn, P. Meredith, Electro-optics of perovskite solar cells, Nat. Photonics. 9 (2015) 106–112. doi:10.1038/nphoton.2014.284.

[25] A. Polman, H.A. Atwater, Photonic design principles for ultrahigh-efficiency photovoltaics, Nat. Mater. 11 (2012) 174–177. doi:10.1038/nmat3263.

[26] M. Karg, T.A.F. König, M. Retsch, C. Stelling, P.M. Reichstein, T. Honold, M. Thelakkat, A. Fery, Colloidal self-assembly concepts for light management in photovoltaics, Mater. Today. 18 (2015) 185–205. doi:10.1016/j.mattod.2014.10.036.

[27] M.L. Brongersma, Y. Cui, S. Fan, Light management for photovoltaics using high-index nanostructures, Nat. Mater. 13 (2014) 451–460. doi:10.1038/nmat3921.

[28] L.C. Andreani, A. Bozzola, P. Kowalczewski, M. Liscidini, Photonic light trapping and electrical transport in thin-film silicon solar cells, Sol. Energy Mater. Sol. Cells. 135 (2015) 78–92. doi:10.1016/J.SOLMAT.2014.10.012.

[29] A. Ingenito, O. Isabella, M. Zeman, Experimental Demonstration of 4 n^2 Classical Absorption Limit in Nanotextured Ultrathin Solar Cells with Dielectric Omnidirectional Back Reflector, ACS Photonics. 1 (2014) 270–278. doi:10.1021/ph4001586.

[30] M.S. Branham, W.-C. Hsu, S. Yerci, J. Loomis, S. V. Boriskina, B.R. Hoard, S.E. Han, A. Ebong, G. Chen, Empirical Comparison of Random and Periodic Surface Light-Trapping Structures for Ultrathin Silicon Photovoltaics, Adv. Opt. Mater. 4 (2016) 858–863. doi:10.1002/adom.201500667.

[31] F.-J. Haug, C. Ballif, Light management in thin film silicon solar cells, Energy Environ. Sci. 8 (2015) 824–837. doi:10.1039/C4EE03346A.

[32] Y. Yang, M. Yang, D.T. Moore, Y. Yan, E.M. Miller, K. Zhu, M.C. Beard, Top and bottom surfaces limit carrier lifetime in lead iodide perovskite films, Nat. Energy. 2 (2017) 16207. doi:10.1038/nenergy.2016.207.

[33] L. Zheng, Y. Ma, S. Chu, S. Wang, B. Qu, L. Xiao, Z. Chen, Q. Gong, Z. Wu, X. Hou,

Improved light absorption and charge transport for perovskite solar cells with rough interfaces by sequential deposition, Nanoscale. 6 (2014) 8171–8176. doi:10.1039/C4NR01141D.

[34] A.R. Pascoe, S. Meyer, W. Huang, W. Li, I. Benesperi, N.W. Duffy, L. Spiccia, U. Bach, Y.-B. Cheng, Enhancing the Optoelectronic Performance of Perovskite Solar Cells via a Textured $CH_3NH_3PbI_3$ Morphology, Adv. Funct. Mater. 26 (2016) 1278–1285. doi:10.1002/adfm.201504190.

[35] B. Shi, B. Liu, J. Luo, Y. Li, C. Zheng, X. Yao, L. Fan, J. Liang, Y. Ding, C. Wei, D. Zhang, Y. Zhao, X. Zhang, Enhanced light absorption of thin perovskite solar cells using textured substrates, Sol. Energy Mater. Sol. Cells. 168 (2017) 214–220. doi:10.1016/J.SOLMAT.2017.04.038.

[36] M. Jošt, S. Albrecht, L. Kegelmann, C.M. Wolff, F. Lang, B. Lipovšek, J. Krč, L. Korte, D. Neher, B. Rech, M. Topič, Efficient Light Management by Textured Nanoimprinted Layers for Perovskite Solar Cells, ACS Photonics. 4 (2017) 1232–1239. doi:10.1021/acsphotonics.7b00138.

[37] D.-L. Wang, H.-J. Cui, G.-J. Hou, Z.-G. Zhu, Q.-B. Yan, G. Su, Highly efficient light management for perovskite solar cells, Sci. Rep. 6 (2016) 18922. doi:10.1038/srep18922.

[38] A. Peer, R. Biswas, J.-M. Park, R. Shinar, J. Shinar, Light management in perovskite solar cells and organic LEDs with microlens arrays, Opt. Express. 25 (2017) 10704. doi:10.1364/OE.25.010704.

[39] H. Wang, B. Cai, X. Yuan, Significant light absorption improvement in perovskite/CIGS tandem solar cells with dielectric nanocone structures, J. Phys. Conf. Ser. 844 (2017) 012004. doi:10.1088/1742-6596/844/1/012004.

[40] N. Horiuchi, Photonic nanojets, Nat. Photonics. 6 (2012) 138–139. doi:10.1038/nphoton.2012.43.

[41] M. Omelyanovich, S. Makarov, V. Milichko, C. Simovski, Enhancement of Perovskite Solar Cells by Plasmonic Nanoparticles, Mater. Sci. Appl. 07 (2016) 836–847. doi:10.4236/msa.2016.712064.

[42] Q. Luo, C. Zhang, X. Deng, H. Zhu, Z. Li, Z. Wang, X. Chen, S. Huang, Plasmonic Effects of Metallic Nanoparticles on Enhancing Performance of Perovskite Solar Cells, ACS Appl. Mater. Interfaces. 9 (2017) 34821–34832. doi:10.1021/acsami.7b08489.

[43] R.T. Ginting, S. Kaur, D.-K. Lim, J.-M. Kim, J.H. Lee, S.H. Lee, J.-W. Kang, Plasmonic Effect of Gold Nanostars in Highly Efficient Organic and Perovskite Solar Cells, ACS Appl. Mater. Interfaces. 9 (2017) 36111–36118. doi:10.1021/acsami.7b11084.

[44] M. Long, Z. Chen, T. Zhang, Y. Xiao, X. Zeng, J. Chen, K. Yan, J. Xu, Ultrathin efficient perovskite solar cells employing a periodic structure of a composite hole conductor for elevated plasmonic light harvesting and hole collection, Nanoscale. 8 (2016) 6290–6299.

doi:10.1039/C5NR05042A.

[45] J. Yin, H. Qu, J. Cao, H. Tai, J. Li, N. Zheng, Light absorption enhancement by embedding submicron scattering TiO_2 nanoparticles in perovskite solar cells, RSC Adv. 6 (2016) 24596–24602. doi:10.1039/C6RA01894G.

[46] Triple-junction thin-film silicon solar cell fabricated on periodically textured substrate with a stabilized efficiency of 13.6%, Appl. Phys. Lett. 106 (2015) 213902. doi:10.1063/1.4921794.

[47] O. Sanchez-Sobrado, M.J. Mendes, S. Haque, T. Mateus, A. Araujo, H. Aguas, E. Fortunato, R. Martins, Colloidal-lithographed TiO_2 photonic nanostructures for solar cell light trapping, J. Mater. Chem. C. 5 (2017) 6852–6861. doi:10.1039/C7TC01756A.

[48] M.J. Mendes, A. Araújo, A. Vicente, H. Águas, I. Ferreira, E. Fortunato, R. Martins, Design of optimized wave-optical spheroidal nanostructures for photonic-enhanced solar cells, Nano Energy. 26 (2016) 286–296. doi:10.1016/J.NANOEN.2016.05.038.

[49] F. Fu, T. Feurer, T.P. Weiss, S. Pisoni, E. Avancini, C. Andres, S. Buecheler, A.N. Tiwari, High-efficiency inverted semi-transparent planar perovskite solar cells in substrate configuration, Nat. Energy. 2 (2016) 16190. doi:10.1038/nenergy.2016.190.

[50] M.I. Hossain, W. Qarony, V. Jovanov, Y.H. Tsang, D. Knipp, Nanophotonic design of perovskite/silicon tandem solar cells, J. Mater. Chem. A. 6 (2018) 3625–3633. doi:10.1039/C8TA00628H.

[51] G.W.P. Adhyaksa, E. Johlin, E.C. Garnett, Nanoscale Back Contact Perovskite Solar Cell Design for Improved Tandem Efficiency, Nano Lett. 17 (2017) 5206–5212. doi:10.1021/acs.nanolett.7b01092.

[52] S.-F. Leung, Q. Zhang, M.M. Tavakoli, J. He, X. Mo, Z. Fan, Progress and Design Concerns of Nanostructured Solar Energy Harvesting Devices, Small. 12 (2016) 2536–2548. doi:10.1002/smll.201502015.

[53] H. Zhang, J. Toudert, Optical management for efficiency enhancement in hybrid organic-inorganic lead halide perovskite solar cells, Sci. Technol. Adv. Mater. 19 (2018) 411–424. doi:10.1080/14686996.2018.1458578.

[54] Y. Yang, J. You, Make perovskite solar cells stable, Nature. 544 (2017) 155–156. doi:10.1038/544155a.

[55] S.N. Habisreutinger, D.P. McMeekin, H.J. Snaith, R.J. Nicholas, Research Update: Strategies for improving the stability of perovskite solar cells, APL Mater. 4 (2016) 091503. doi:10.1063/1.4961210.

[56] S.M. Kang, N. Ahn, J.-W. Lee, M. Choi, N.-G. Park, Water-repellent perovskite solar cell, J. Mater. Chem. A. 2 (2014) 20017–20021. doi:10.1039/C4TA05413J.

[57] E. Yablonovitch, G.D. Cody, Intensity enhancement in textured optical sheets for solar cells, IEEE Trans. Electron Devices. 29 (1982) 300–305. doi:10.1109/T-ED.1982.20700.

[58] M.A. Green, Lambertian light trapping in textured solar cells and light-emitting diodes: analytical solutions, Prog. Photovoltaics Res. Appl. 10 (2002) 235–241. doi:10.1002/pip.404.

[59] A. Bozzola, M. Liscidini, L.C. Andreani, Photonic light-trapping versus Lambertian limits in thin film silicon solar cells with 1D and 2D periodic patterns, Opt. Express. 20 (2012) A224. doi:10.1364/OE.20.00A224.

[60] FDTD Solutions | Lumerical's Nanophotonic FDTD Simulation Software, (n.d.). https://www.lumerical.com/tcad-products/fdtd/ (accessed March 7, 2018).

[61] M.G. Deceglie, V.E. Ferry, A.P. Alivisatos, H.A. Atwater, Design of Nanostructured Solar Cells Using Coupled Optical and Electrical Modeling, Nano Lett. 12 (2012) 2894–2900. doi:10.1021/nl300483y.

[62] L. Qiu, J. Deng, X. Lu, Z. Yang, H. Peng, Integrating Perovskite Solar Cells into a Flexible Fiber, Angew. Chemie Int. Ed. 53 (2014) 10425–10428. doi:10.1002/anie.201404973.

[63] K.J. Yu, L. Gao, J.S. Park, Y.R. Lee, C.J. Corcoran, R.G. Nuzzo, D. Chanda, J.A. Rogers, Light Trapping in Ultrathin Monocrystalline Silicon Solar Cells, Adv. Energy Mater. 3 (2013) 1401–1406. doi:10.1002/aenm.201300542.

[64] J. Nam, Y. Lee, W. Choi, C.S. Kim, H. Kim, J. Kim, D.-H. Kim, S. Jo, Transfer Printed Flexible and Stretchable Thin Film Solar Cells Using a Water-Soluble Sacrificial Layer, Adv. Energy Mater. 6 (2016) 1601269. doi:10.1002/aenm.201601269.

[65] H. Águas, T. Mateus, A. Vicente, D. Gaspar, M.J. Mendes, W.A. Schmidt, L. Pereira, E. Fortunato, R. Martins, Thin Film Silicon Photovoltaic Cells on Paper for Flexible Indoor Applications, Adv. Funct. Mater. 25 (2015) 3592–3598. doi:10.1002/adfm.201500636.

[66] M. Karg, T.A.F. König, M. Retsch, C. Stelling, P.M. Reichstein, T. Honold, M. Thelakkat, A. Fery, Colloidal self-assembly concepts for light management in photovoltaics, Mater. Today. 18 (2015) 185–205. doi:10.1016/J.MATTOD.2014.10.036.

[67] U. Mehmood, A. Al-Ahmed, M. Afzaal, F.A. Al-Sulaiman, M. Daud, Recent progress and remaining challenges in organometallic halides based perovskite solar cells, Renew. Sustain. Energy Rev. 78 (2017) 1–14. doi:10.1016/j.rser.2017.04.105.

[68] H. Uratani, K. Yamashita, Charge Carrier Trapping at Surface Defects of Perovskite Solar Cell Absorbers: A First-Principles Study, J. Phys. Chem. Lett. 8 (2017) 742–746. doi:10.1021/acs.jpclett.7b00055.

[69] Y. Sun, X. Fang, Z. Ma, L. Xu, Y. Lu, Q. Yu, N. Yuan, J. Ding, Enhanced UV-light stability of organometal halide perovskite solar cells with interface modification and a UV absorption layer, J. Mater. Chem. C. 5 (2017) 8682–8687. doi:10.1039/C7TC02603J.

[70] L. Jiang, W. Chen, J. Zheng, L. Zhu, L. Mo, Z. Li, L. Hu, T. Hayat, A. Alsaedi, C. Zhang, S. Dai, Enhancing the Photovoltaic Performance of Perovskite Solar Cells with a Down-Conversion Eu-Complex, ACS Appl. Mater. Interfaces. 9 (2017) 26958–26964.

doi:10.1021/acsami.7b10101.

[71] J. Jin, H. Li, C. Chen, B. Zhang, W. Bi, Z. Song, L. Xu, B. Dong, H. Song, Q. Dai, Improving Efficiency and Light Stability of Perovskite Solar Cells by Incorporating $YVO_4:Eu^{3+}$, Bi^{3+} Nanophosphor into the Mesoporous TiO_2 Layer, ACS Appl. Energy Mater. 1 (2018) 2096–2102. doi:10.1021/acsaem.8b00192.

[72] Y. Zhang, Y. Xu, S. Chen, H. Lu, K. Chen, Y. Cao, A.E. Miroshnichenko, M. Gu, X. Li, Ultra-Broadband Directional Scattering by Colloidally Lithographed High-Index Mie Resonant Oligomers and Their Energy-Harvesting Applications, ACS Appl. Mater. Interfaces. 10 (2018) 16776–16782. doi:10.1021/acsami.8b03718.

[73] M.M. Tavakoli, K.-H. Tsui, Q. Zhang, J. He, Y. Yao, D. Li, Z. Fan, Highly Efficient Flexible Perovskite Solar Cells with Antireflection and Self-Cleaning Nanostructures, ACS Nano. 9 (2015) 10287–10295. doi:10.1021/acsnano.5b04284.